Atmospheric and Oceanic Science Letters 16 (2023) 100405

Contents lists available at ScienceDirect

Atmospheric and Oceanic Science Letters

journal homepage: www.keaipublishing.com/en/journals/atmospheric-and-oceanic-science-letters/

Impacts of the extratropical North Pacific on boreal summer Arctic circulation

Shengping He [a,b,d,*], Tore Furevik [b,a], Huijun Wang [c,d,e], Fei Li [a], Mingkeng Duan [c]

[a] Geophysical Institute, University of Bergen and Bjerknes Centre for Climate Research, Bergen, Norway
[b] Nansen Environmental and Remote Sensing Center, Bergen, Norway
[c] Key Laboratory of Meteorological Disaster, Ministry of Education/Joint International Research Laboratory of Climate and Environment Change (ILCEC)/Collaborative Innovation Center on Forecast and Evaluation of Meteorological Disasters (CIC-FEMD), Nanjing University of Information Science & Technology, Nanjing, China
[d] Nansen-Zhu International Research Center, Institute of Atmospheric Physics, Chinese Academy of Sciences, Beijing, China
[e] Southern Marine Science and Engineering Guangdong Laboratory (Zhuhai), Zhuhai, China

ARTICLE INFO

Keywords:
Arctic warming
North Pacific
Teleconnection
Eady growth rate
Beaufort Sea
WACCM

ABSTRACT

A distinct characteristic of the Arctic summer atmospheric circulation is the anomalous anticyclonic circulation centered over the Arctic Ocean associated with significant Arctic warming. Previous studies have related the underlying mechanisms to the earlier spring Eurasian snowmelt and the tropical Pacific forcing. Here, the authors show that the Arctic summer anomalous anticyclonic circulation is significantly related to the extratropical North Pacific sea surface temperature anomalies (SSTAs) in spring, indicating a teleconnection from the extratropical North Pacific to the Arctic. The SSTA pattern is characterized by warm anomalies in the midlatitudes of the extratropical North Pacific surrounded by significant cold anomalies, resembling the negative phase of the Pacific Decadal Oscillation (PDO) but without significant signals in the tropics (referred to as the negative PDO-like pattern). This negative PDO-like pattern in May can stimulate a Rossby wave propagating from the Bering Sea to the Arctic and lead to an anomalous Arctic anticyclone which can be sustained during summer. Meanwhile, the negative PDO-like pattern can persist to summer and induce an anomalous surface low pressure over the Bering Sea in summer. This anomalous surface low causes anomalous rising motions and induces upper-level divergence anomalies which further intensify the summer Arctic anticyclone. The upper-level tropospheric Arctic anticyclone can force anomalous adiabatic descent over the Arctic and sub-Arctic, leading to significant adiabatic heating in the Arctic. As a result, a significant warming emerges over the Arctic with the center located in the middle troposphere. The connection between the negative PDO-like SSTAs and the summer Arctic anticyclone has been confirmed by numerical experiments.

关键词:
北极增暖
北太平洋
遥相关
Eady增长率
波弗特海
WACCM

摘 要

北极夏季大气环流的一个显着特征是以北冰洋为中心的异常反气旋环流，与北极增暖存在紧密的联系. 先前的研究已将其形成的潜在机制与早春欧亚融雪，热带太平洋海表温度异常联系起来. 本研究发现北极夏季反气旋环流异常与春季副热带北太平洋海表温度异常 (SSTA) 存在显着联系，表明副热带北太平洋与北极之间存在遥相关. 该SSTA的特点是北太平洋中纬度地区有暖的SSTA，周围有明显的冷SSTA，类似于太平洋年代际振荡 (PDO) 的负位相，但热带地区没有明显的信号 (本研究称之为类负位相PDO) . 5 月份，这种类负位相PDO可以激发从白令海传播到北极的罗斯贝波，导致北极出现反气旋环流异常. 这种反气旋环流异常可以持续到夏季. 同时，这种类负位相PDO的SSTA可以持续到夏季，并在夏季引起白令海上空的低压异常. 这种低层的低压异常会导致异常的上升运动，并引起高层的辐散异常，从而进一步加剧夏季北极对流层上层的反气旋环流异常. 这种反气旋环流异常可迫使北极上空出现异常绝热下沉运动，导致北极出现显著的绝热加热.于是，北极上空出现显著的暖异常，其暖中心位于北极对流层中部. 数值模拟试验证实了5月份类负位相PDO的SSTA与夏季北极反气旋环流异常之间的联系.

* Corresponding author.
E-mail address: Shengping.He@uib.no (S. He).

https://doi.org/10.1016/j.aosl.2023.100405
Received 4 June 2023; Received in revised form 18 July 2023; Accepted 4 August 2023
Available online 5 August 2023
1674-2834/© 2023 The Authors. Publishing Services by Elsevier B.V. on behalf of KeAi Communications Co. Ltd. This is an open access article under the CC BY-NC-ND license (http://creativecommons.org/licenses/by-nc-nd/4.0/).

1. Introduction

The rapid climate change over the Arctic in recent decades is characterized by notable Arctic sea-ice decline and atmospheric and oceanic warming (Gerber et al., 2014; McCusker et al., 2016; Collow et al., 2017; Lind et al., 2018). It is suggested that both natural and anthropogenic drivers have contributed to the changes (Stroeve et al., 2007; Serreze and Barry, 2011; Day et al., 2012; Ding et al., 2017; Dai et al., 2019). The Fifth and Sixth Assessment Reports of the Intergovernmental Panel on Climate Change have highlighted the interlinks between human-induced climate change and the Arctic sea-ice decline over the past few decades (IPCC, 2013, 2022). The Arctic September sea-ice extent for 2007−2022 shows a near-zero trend (Swart et al., 2015; Lindsey and Scott, 2022), which seems to be inconsistent with the continuous strengthening of anthropogenic forcing. Such a paradox may be caused by internal climate variability, which can mask human-induced sea-ice decline associated with a strong anthropogenic forcing (Swart et al., 2015; Xu et al., 2022b). It is well-recognized that natural variability, such as Pacific Decadal Oscillation (Trenberth et al., 2014; Svendsen et al., 2018) and Atlantic Multidecadal Oscillation (Chylek et al., 2009; Day et al., 2012) can drive climate variations in the global and Arctic climate. Model simulations suggest that sea surface temperature (SST) variability outside the Arctic has been the dominant contributor to the recently observed Arctic warming aloft (Screen et al., 2012; Xu et al., 2022a).

Apart from the natural and anthropogenic forcing discussed in the cited studies above, the influence of atmospheric circulation on Arctic sea-ice variability has been investigated extensively (Hu et al., 2002; Rigor et al., 2002; Zhang et al., 2003; Ogi and Wallace, 2007; Deser and Teng, 2008; Zhang et al., 2008; Overland and Wang, 2010; Knudsen et al., 2015; Ding et al., 2017, 2022). Hu et al. (2002) suggested that the upward trend in the North Atlantic Oscillation may underlie the decline of Arctic summer sea-ice extent observed during the 1980s and 1990s. Ogi and Wallace (2007) showed that years with lower Arctic summer sea-ice extent for the period 1979–2006 tend to be associated with anomalous high sea level pressure (SLP) and an anticyclonic circulation over the Arctic in summer. The impact of positive summer SLP anomalies extending from the Beaufort Sea to the Greenland on the Arctic summer sea ice has been documented in several studies (Watanabe et al., 2006; Serreze and Barrett, 2008; Overland et al., 2012). Ding et al. (2017) indicated that about 60% of the Arctic sea-ice decline since 1979 could be attributed to the positive trend of summer atmospheric circulation over Greenland and the Arctic Ocean.

Some studies have explored how the anomalous atmospheric circulation over the Arctic in summer is formed. It has been revealed that the anomalous high pressure over the Beaufort Sea in summer relates to a reduction of cyclogenesis (Moore, 2012; Knudsen et al., 2015). Remote land surface forcing such as earlier spring snowmelt over Eurasia can lead to anomalously positive SLP anomaly over the Arctic in summer via amplifying stationary Rossby waves (Matsumura et al., 2014). Atmospheric model experiments indicate that the tropical Pacific SST may induce the positive trend of upper-tropospheric geopotential height over Greenland and the Arctic Ocean by stimulating a northeastward propagating Rossby wave train (Ding et al., 2014). Svendsen et al. (2018) found that the extratropical North Pacific SST may cause winter Arctic warming. These studies imply a potential influence of natural variability on the Arctic atmospheric circulation. The question of whether changes in boreal summer Arctic atmospheric circulation can be forced by extratropical North Pacific SST has, however, not been examined.

In this study, we examine the potential contribution of the extratropical North Pacific SST to the Arctic boreal summer (June–July–August, JJA) atmospheric circulation anomalies.

2. Data and methods

Monthly SST on a 1° × 1° grid was obtained from the Hadley Centre Sea Ice and Sea Surface Temperature dataset, version 1 (HadISST1) (Rayner et al., 2003). Reanalysis data were obtained from the NCEP/-DOE Reanalysis II (Kanamitsu et al., 2002) with a 2.5° × 2.5° horizontal resolution. NCEP/DOE Reanalysis II is an improved version of the NCEP Reanalysis I model with error corrections and updated parameterizations of physical processes. We focus on the results post-1979, since the analyses of geopotential height and other variables over the Northern Hemisphere polar region, especially those in the upper troposphere, are more reliable during the modern satellite era (Bromwich et al., 2007). All the regression and correlation results are based on detrended datasets. A diagnostic for cyclogenesis is the Eady growth rate (EGR, σ). This indicates the baroclinic instability to the vertical wind shear and static stability (Lindzen and Farrell, 1980), and is defined as

$$\sigma = 0.3098 \frac{|f| \left| \frac{\partial U(z)}{\partial z} \right|}{N},$$

where f is the Coriolis parameter; N is the Brunt–Väisällä frequency, defined by $N^2 = \frac{g}{\theta} \frac{\partial \theta}{\partial z}$, in which g is the acceleration due to gravity, z is the vertical coordinate, and θ is the potential temperature; and $U(z)$ is the vertical profile of the eastward wind component. Higher EGR means a stronger instability (Serreze and Barrett, 2008), leading to more generations of cyclogenesis.

3. Results

3.1. Covariance between the Arctic and the North Pacific

Previous studies have shown that the Arctic summer atmospheric circulation displays notable changes associated with the Arctic climate change (Serreze and Barrett, 2011; Ding et al., 2014, 2017). To represent the main pattern of tropospheric circulation over the Arctic in summer, we applied empirical orthogonal analysis (EOF) to the 200-hPa geopotential height (Z200). The time series of the first principal component is referred to as Z200-EOF-PC1. This is the same level as was used by Ding et al. (2017), who suggested that the positive trend of summer Z200 over northeastern Canada and Greenland has a pronounced influence on the temperature, humidity, and downward longwave radiation over the Arctic in summer, contributing to a reduction in sea ice.

The dominant pattern of the Arctic summer Z200 anomaly is characterized by a notable center over the Arctic Ocean extending to Greenland (Fig. 1(a)). The first leading mode of EOF (EOF1) explains about 53.3% of the total variance of the Arctic summer Z200 anomaly. This feature is consistent with the atmospheric circulation anomaly emerging in the summer of 2007, which exerted a pronounced reduction in Arctic sea ice and enhanced temperatures (Serreze and Barrett, 2011), and resembles well the Arctic summer SLP anomalies associated with the reduction of Arctic summer sea-ice extent (Ogi and Wallace, 2007; Knudsen et al., 2015). The Z200 anomalies are closely related to the intensity of the Arctic summer cyclonic activity (Serreze and Barrett, 2008). The principal component of EOF1 for summer Z200 (Z200-EOF-PC1) shows a close relationship with the variability of the summer Z200 anomaly averaged over Greenland (66°–80°N, 50°W–0°; referred to as GL-Z200) (Ding et al., 2017). Namely, the original (detrended) Z200-EOF-PC1 and GL-Z200 are correlated at $r = 0.89$ (0.84). Therefore, Z200-EOF-PC1 can be used to describe the variability of boreal summer atmospheric circulation over the Arctic.

The statistically significant summer atmospheric circulation anomalies (geopotential height and zonal wind) related to the Z200-EOF-PC1 exhibit a barotropic structure throughout the Arctic troposphere but do not extend to the North Pacific (not shown). The summer Z200 anomalies and the associated wave activity flux (WAF) are mainly confined to the Arctic (Fig. 1(b)), and no significant WAF is found to propagate from the Pacific to the Arctic. This is different from the conclusions of Ding et al. (2014), who pointed out that the positive trend of annual mean Z200 over Greenland and the Arctic is strongly associated with Rossby

wave-train activity originating from the tropical Pacific. The contrasting results may be related to the different time scale used in the studies. Interestingly, the anomalies of Arctic summer Z200 are associated with significant geopotential height anomalies and WAF in the spring months (e.g., May) (Fig. 1(a)). Significant positive and negative 500-hPa geopotential height anomalies emerge over the extratropical North Pacific and east of the Bering Sea in spring, respectively (Fig. 1(a), contours). The corresponding WAF originates from the extratropical North Pacific, which exhibits a distinctive arc-shaped trajectory and propagates northeastwards through Canada (Fig. 1(a), vectors). Notably, the poleward propagating wave activity is observed over the North Pacific in both March and April. However, such a feature is more dominant in May during which the wave activity originating from the extratropical North Pacific propagates poleward to the Arctic (Fig. 1(a), vectors). The atmospheric circulation anomalies are marked by significant positive, negative, and positive geopotential height anomalies over the Arctic, the Bering Sea, and the extratropical North Pacific, respectively (Fig. 1(a), contours), which display a barotropic structure throughout the troposphere (figure not shown). Based on the apparent poleward wave activity originating from the extratropical North Pacific in May (Fig. 1(a)), and motivated by a recent study by Lapointe et al. (2017) who implied the potential impacts of the PDO on the climate over the western Canadian Arctic, we hypothesize that the extratropical North Pacific SST in May can play an important role in modulating the Arctic summer climate.

Our hypothesis that the Arctic summer geopotential height anomalies have a significant relationship with the spring North Pacific SST is supported by maximum covariance analysis (MCA). The first leading mode of covariability between the Arctic summer Z200 and May SST in the North Pacific for 1979−2022 is shown in Fig. 2. The first leading MCA explains 82.4% of the covariance between the Arctic summer Z200 and May SST in the North Pacific. The MCA pattern of Arctic summer Z200 shows a distinct anomalous center confined over the Arctic (Fig. 2 (a)), consistent with the corresponding EOF1 pattern (Fig. 1(b)). It suggests that associated with positive Z200 anomalies over the Arctic in summer, the May SST exhibits significant positive anomalies centered at midlatitudes (around 30°–40°N) of the extratropical North Pacific, surrounded by negative anomalies (Fig. 2(b)). Note that the SSTAs in the tropical Pacific are barely significant. The time series associated with the first MCA mode (MCA1) is significantly correlated, with a correlation coefficient of 0.52 (Fig. 2(c)). Thus, the leading SSTA pattern in the extratropical North Pacific, which resembles the PDO (Mantua et al., 1997), may contribute to the Arctic summer atmospheric circulation anomalies. We call this SST pattern a negative PDO-like pattern for short.

3.2. Mechanisms of the North Pacific–Arctic teleconnection

To represent the variability of the PDO-like SSTAs shown in Fig. 2(b), we define an extratropical North Pacific (ENP) SST index (ENPSSTI). The ENPSSTI is defined as the difference of the area-averaged ENP SST over the areas with significant positive values in Fig. 2(b) from the area-averaged ENP SST over the areas with significant negative values in Fig. 2(b) (north of 20°N, 120°E–100°W). Considering the weak signals in the tropical Pacific, we removed the influence of El Niño–Southern Oscillation in advance when we defined the ENPSSTI, by removing the variability associated with the SSTAs in the Niño3.4 region using linear regression. To emphasize the impact of extratropical ENP SST on the Arctic atmosphere, we choose the ENPSSTI in May, which leads the variations of the Arctic atmosphere in summer.

Focusing on the North Pacific-Arctic sector (180°–150°W), we show the geopotential height variance and WAF (Takaya and Nakamura, 2001) associated with May ENPSSTI in Fig. 3(a–c) as two-month running means. Rossby wave fluxes, which originate from the ENP (50°–60°N), propagate poleward during May–June (Fig. 3(a), vectors), suggesting the potential forcing of the ENP SSTAs. This feature can also be seen in the horizontal propagation of the WAF in May (Fig. 3(d)). The poleward Rossby wave fluxes have not been sustained in June–July (Fig. 3(b, d), vectors) and July–August (Fig. 3(c, f), vectors); however, the high anomalies over the Arctic are sustained and developed from May to August (Fig. 3(d–f), contours), further indicating the influence of May ENP SSTAs. This is consistent with the results revealed in Fig. 1, which shows a poleward propagation of horizontal wave activities from the east of the Bering Sea to the Beaufort Sea in May. It confirms the lagging change in the atmosphere over the Arctic. There is a clear continuous intensification of positive geopotential height anomalies from May to August over the Arctic (Fig. 3(a–c), shading). From the daily evolution of the geopotential height variance, the anomalies associated with the May ENPSSTI start to propagate from the extratropical NP poleward toward the Arctic around mid-May and then are sustained until the end of August (figure not shown).

We now examine the possible mechanisms that may explain the dynamical response of the Arctic summer atmosphere to the ENP SSTAs. Moore (2012) suggested that the negative trend of EGR in the Beaufort

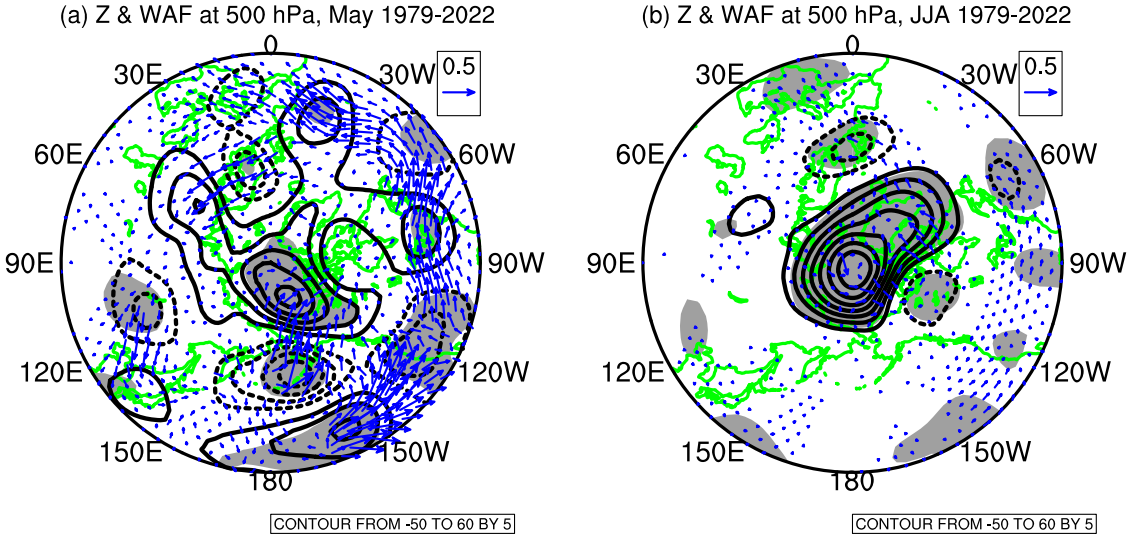

Fig. 1. Teleconnections from the North Pacific to the Arctic. Geopotential height anomalies (Z; contours with intervals of 5; units: gpm) and associated WAF (vectors; units: $m^2\ s^{-2}$) at 500 hPa in (a) May and (b) June–August during 1979–2022 (north of 30°N) regressed onto the detrended and normalized JJA Z200-EOF-PC1. Shading indicates regions with height anomalies statistically significant at the 0.05 level.

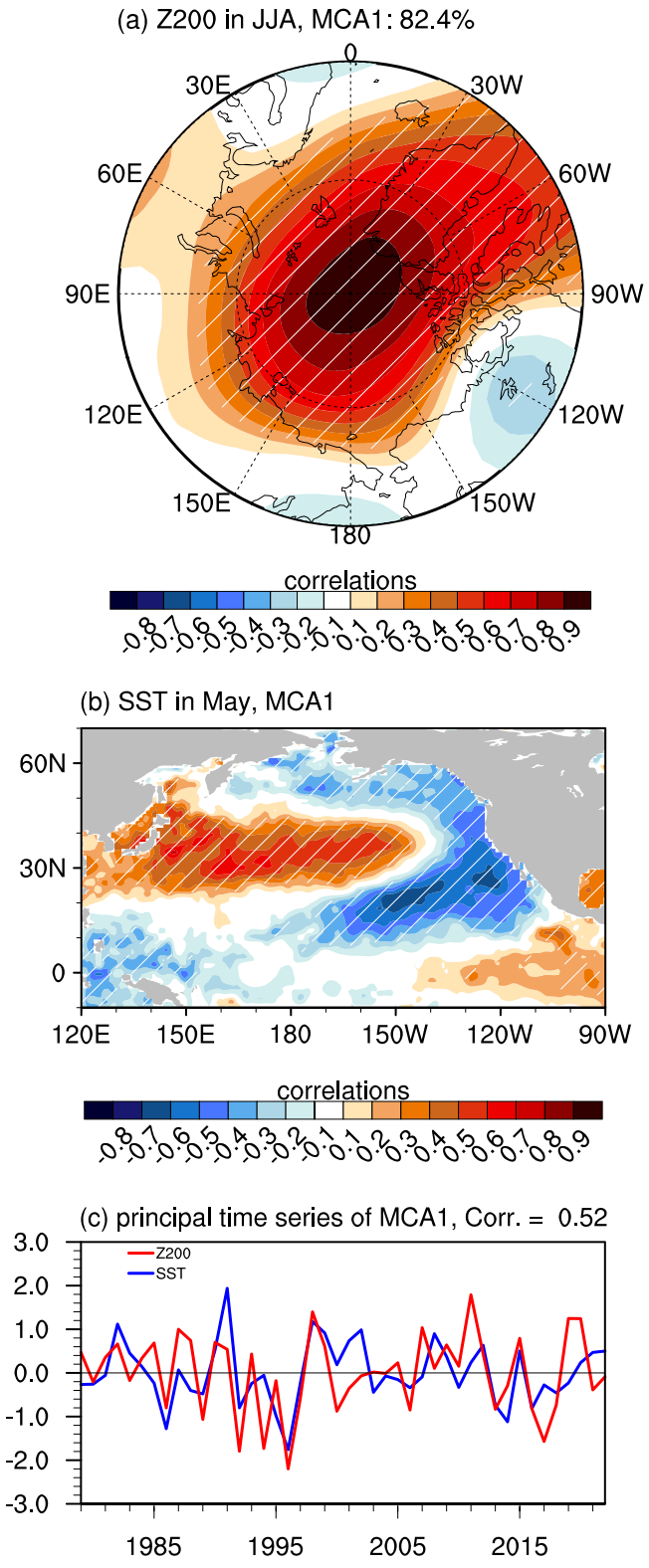

Fig. 2. Covariance between the North Pacific SST and the Arctic circulation. Results of MCA for 200-hPa geopotential height north of 70°N in JJA and subtropical North Pacific (20°–70°N, 120°E–120°W) SST in May for 1979–2022. Hatching indicates coefficients statistically significant at the 0.05 level. Shown in (a) are the patterns of Z200 (shading) and (b) SST (shading) that accompany the first mode. (c) Time series of the Z200 (red) and SST (blue) patterns shown in (a) and (b). Shading indicates correlation coefficients with the first mode of MCA.

Sea may contribute to the positive trend of the summer Beaufort Sea High. Therefore, we present, in Fig. 4(d–f), the regression of the two-month running mean of EGR from May to August onto the May ENPSSTI. A clear consequence of the positive May ENPSSTI is the significant negative EGR anomalies over the Arctic which appear over the Beaufort Sea in May–June and expand to the entire Arctic in July–August (Fig. 4(d–f)). It means a significant reduction of the Arctic baroclinicity in summer associated with the SSTA pattern in May shown in Fig. 2(b). These negative EGR anomalies can cause a reduction of cyclogenesis and lead to anomalous high pressure over the Beaufort Sea (Moore, 2012; Knudsen et al., 2015) (Fig. 4(a, b)). The reduced baroclinicity from May to August relates to the weakening of the meridional temperature gradient over the Beaufort Sea (i.e., positive dT/dy in Fig. 4 (g–i) , T is the air temperature with unit in K and y is the latitude with uint in km), induced by the persistent significantly negative SSTAs near the Bering Sea (Fig. 2(b)). This supports the earlier findings by Peings and Magnusdottir (2014). As a result, the zonal wind over the Arctic-Pacific sector shows significantly negative zonal wind anomalies with the maximum magnitude center over the Beaufort Sea (Fig. 4 (j–l)). The negative zonal wind anomalies emerging over the Beaufort Sea in May–June are sustained to August with a gradual intensification. Meanwhile, significantly negative zonal wind anomalies extend from the North Atlantic northeastward into the Barents Seas, consistent with the pathway of the primary North Atlantic storm track (Serreze and Barrett, 2008). These zonal wind anomalies may also be related to the ENP SSTAs which can simulate Rossby wave activities propagating to the North Atlantic (Fig. 3(d, e)).

Accompanied by the deceleration of the circumpolar westerly wind at high latitudes (see the Beaufort Sea and Barents Sea in Fig. 4(j–l)), statistically significant positive 200-hPa geopotential height anomalies are centered over the Arctic Ocean (Fig. 5(a)) with an equivalent barotropic structure in the troposphere (figure not shown). The anomalous anticyclonic circulation aloft over the Arctic can force anomalous adiabatic descent which contributes to the Arctic warm anomalies (Ding et al., 2017). Additionally, the negative PDO-like SSTA pattern (see Fig. 2(b) can induce an anomalous surface low pressure over the Bering Sea which can cause anomalous rising motions aloft and anomalous subsidence over the Arctic and/or the sub-Arctic (figure not shown), leading to warmer anomalies in the Arctic troposphere due to adiabatic heating (Matsumura et al., 2014). To further examine the connection between the SSTAs and the Arctic temperature, we further analyze the relationship between the May ENPSSTI and the Arctic summer air temperature. Significant warm anomalies emerge in the troposphere over the Arctic. It should be noted that the terminus of the Arctic tropospheric warm anomalies is below 200 hPa with a center located in the middle troposphere (Fig. 5(c, f)) which is lower than that of positive geopotential height anomalies (Fig. 3(b, c), shading), confirming that the significant boreal summer Arctic warming is caused by the dominant tropospheric circulation in the Arctic rather than by the Arctic sea ice.

To round off the discussion on the influence of the ENP SSTAs on the Arctic atmospheric circulation and temperature, we use the Whole Atmosphere Community Climate Model (WACCM; Marsh et al., 2013) to perform numerical simulations, setting sea-ice concentration and SST as boundary conditions and all other external variables fixed. One control experiment is forced by the seasonally varying climatological (1979–2000) sea-ice concentration and SST. Subsequently, a pair of 12-month sensitivity experiments from January to December are performed, with SSTA perturbations in the ENP from May to August (as indicated by the significant correlations in Fig. 2(b), north of 20°N) while other months are prescribed with climatological SST. The sensitivity (control) experiments were integrated over 60 (40) years, and the first 10 years of data were omitted before analysis. The difference between the sensitivity and control experiments in summer is presented to illustrate the response of the atmosphere to the ENP SSTAs which start in May. The difference in the summer atmosphere between the sensitivity and control experiments is characterized by significant positive 200-hPa

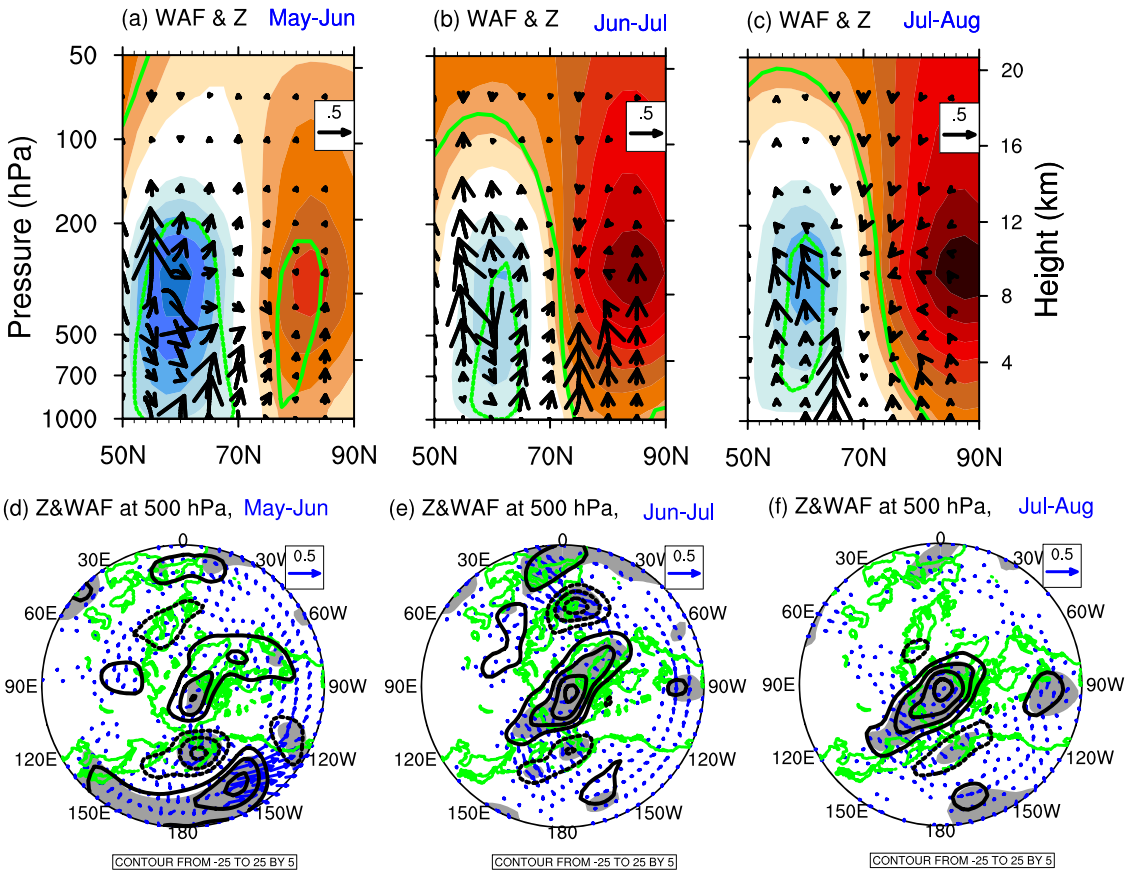

Fig. 3. Rossby waves propagating from the North Pacific to the Arctic. Geopotential height anomalies (shading; units: gpm) zonally averaged over 180°–150°W in (a) May–June, (b) June–July, and (c) July–August for 1979–2022 regressed onto the detrended and normalized May ENPSSTI; vectors are the associated WAF (units: $m^2\ s^{-2}$). Regions enclosed by green contours indicate height anomalies statistically significant at the 0.05 level.

geopotential height anomalies over the Arctic Ocean (Fig. 5(d)). Compared to the observed counterpart (Fig. 5(a)), the positive anomaly center shifts slightly southward to the Beaufort Sea and the magnitude of the negative anomaly over the Barents Sea is larger. Similar to the observations, the simulated 700-hPa air temperature shows positive anomalies from northern Siberia across the Arctic Ocean to Greenland, with the significant positive anomaly center located near the Beaufort Sea (Fig. 5(e)). Interestingly, the simulated warm anomalies are mainly confined to the Arctic (north of 70°N) and below 200 hPa (Fig. 5(f)), which also resembles the observations. We note that the WACCM, forced by the ENP SSTAs from May to August, has reproduced the poleward Rossby waves propagating from the Bering Sea to the Arctic (figure not shown). Overall, the simulated summer Arctic atmospheric anomalies closely resemble the observed counterparts associated with the negative PDO-like SSTAs which persist from May to August, confirming that the ENP SSTAs can influence the Arctic atmospheric temperature and circulation in summer.

4. Conclusions

In this paper, we present a mechanism linking the extratropical North Pacific to the boreal summer Arctic atmospheric circulation and temperature variability. The Arctic summer atmospheric circulation is characterized by a prominent maximum variance center over the Arctic Ocean with an equivalent barotropic structure in the troposphere. Concurrent with this feature, the North Pacific SST shows significant positive anomalies in the midlatitudes (30°–40°N), surrounded by anomalies with opposite signs, resembling the PDO pattern but without clear linkages to the tropical Pacific. Observational analyses suggest that the negative SSTAs in the Bering Sea shown in Fig. 2(b) can weaken the meridional temperature gradient from the Bering Sea to the Beaufort Sea, leading to a weaking of atmospheric baroclinic instability over the Arctic, especially in the Beaufort Sea. It can cause a reduction of cyclogenesis and lead to anomalous high pressure over the Beaufort Sea (Moore, 2012; Knudsen et al., 2015). The PDO-like SSTAs can simulate a Rossby wave teleconnection from the North Pacific to the Arctic, leading to positive geopotential height anomalies in the Arctic. Consequently, an anomalous anticyclone emerges in the upper troposphere over the Arctic, which causes anomalous subsidence over the Arctic and/or the sub-Arctic. The anomalous subsidence induces significant adiabatic heating, leading to significant Arctic tropospheric warming. The WACCM, which is perturbed by negative PDO-like SSTAs in the extratropical North Pacific from May to August with the influence of El Niño-Southern Oscillation having been removed, reproduced the observed positive geopotential height anomalies and tropospheric warm anomalies over the Arctic in summer.

Many studies have noted the distinct features of the Arctic summer atmospheric circulation, such as the summer cyclone maximum (Serreze and Barrett, 2008), the Beaufort Sea high (Serreze and Barrett, 2011; Moore, 2012), and the anomalous anticyclonic circulation over Greenland (Ding et al., 2017). However, our understanding of the contributing factors to the Arctic summer atmospheric variability is far from complete. Serreze and Barrett (2008) suggested the effect of the cyclogenesis over the Arctic Ocean and the influx of lows generated over the Eurasian continent. Matsumura and Yamazaki (2012) revealed that the earlier spring Eurasian snowmelt can lead to anomalous anticyclonic circulation over the Arctic Ocean by amplifying the propagation of the stationary Rossby waves. Additionally, a few studies have revealed the potential teleconnection between the tropical Pacific and high latitudes (Trenberth et al., 2014) and the Arctic (Ding et al., 2014). However,

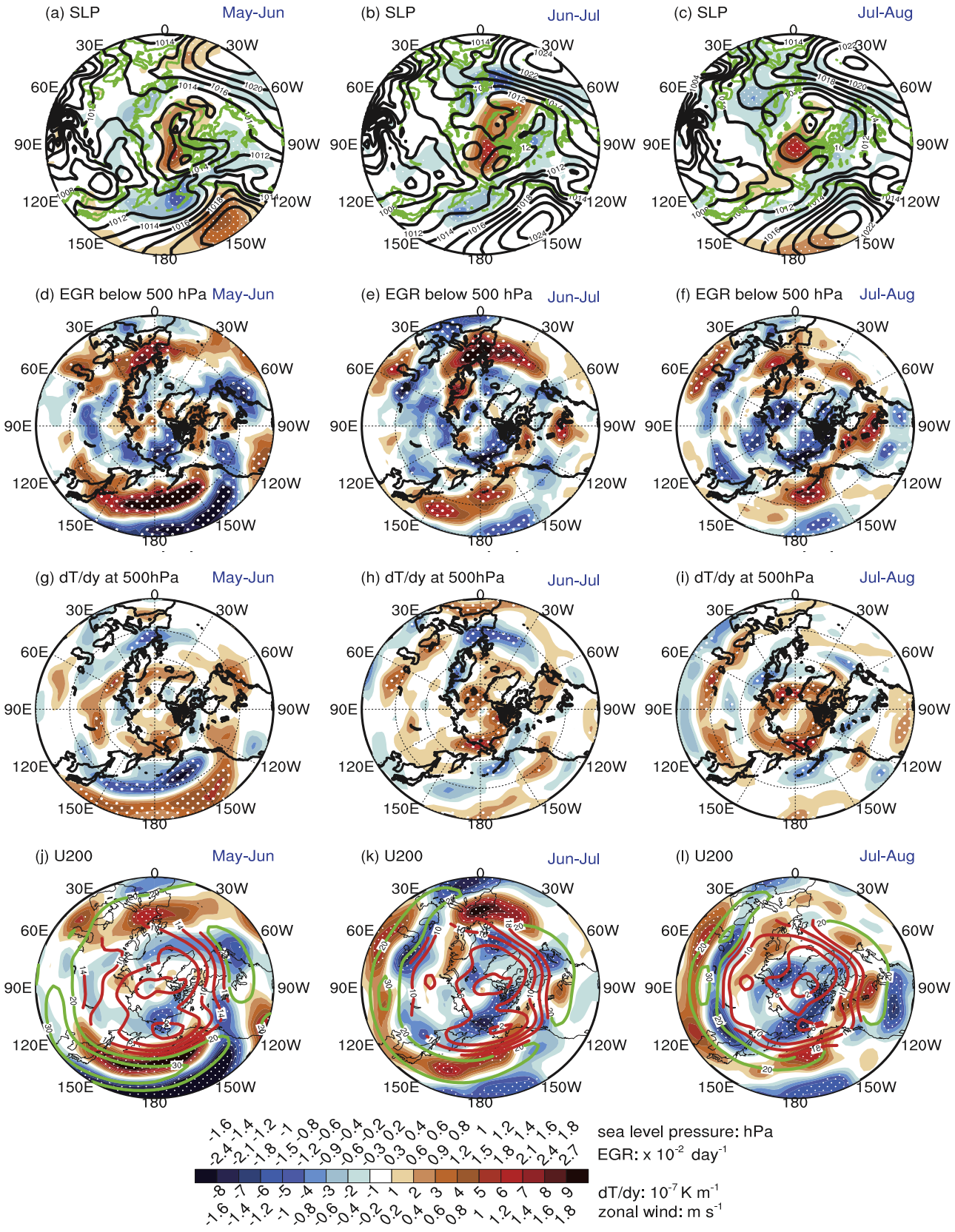

Fig. 4. Impacts of North Pacific SST on high-latitude atmospheric circulation. SLP anomalies (shading) in (a) May–June, (b) June–July, and (c) July–August for 1979–2022 regressed onto the detrended and normalized May ENPSSTI; its climatology is shown by contours with intervals of 2 (units: hPa). Panels (d, g, j), (e, h, k), and (f, i, l) are the same as (a–c), respectively, but for the EGR calculated from the surface to 500 hPa (shading; units: $\times 10^{-2}$ d^{-1}), 500-hPa temperature meridional gradient ($\partial T/\partial y$; shading; units: $\times 10^{-7}$ K m^{-1}; positive values indicates that the temperature anomalies increase poleward), and zonal wind at 200 hPa (U200; shading indicates the anomalies and contours indicate the climatology; units: m s^{-1}). Stippled regions indicate anomalies statistically significant at the 0.05 level.

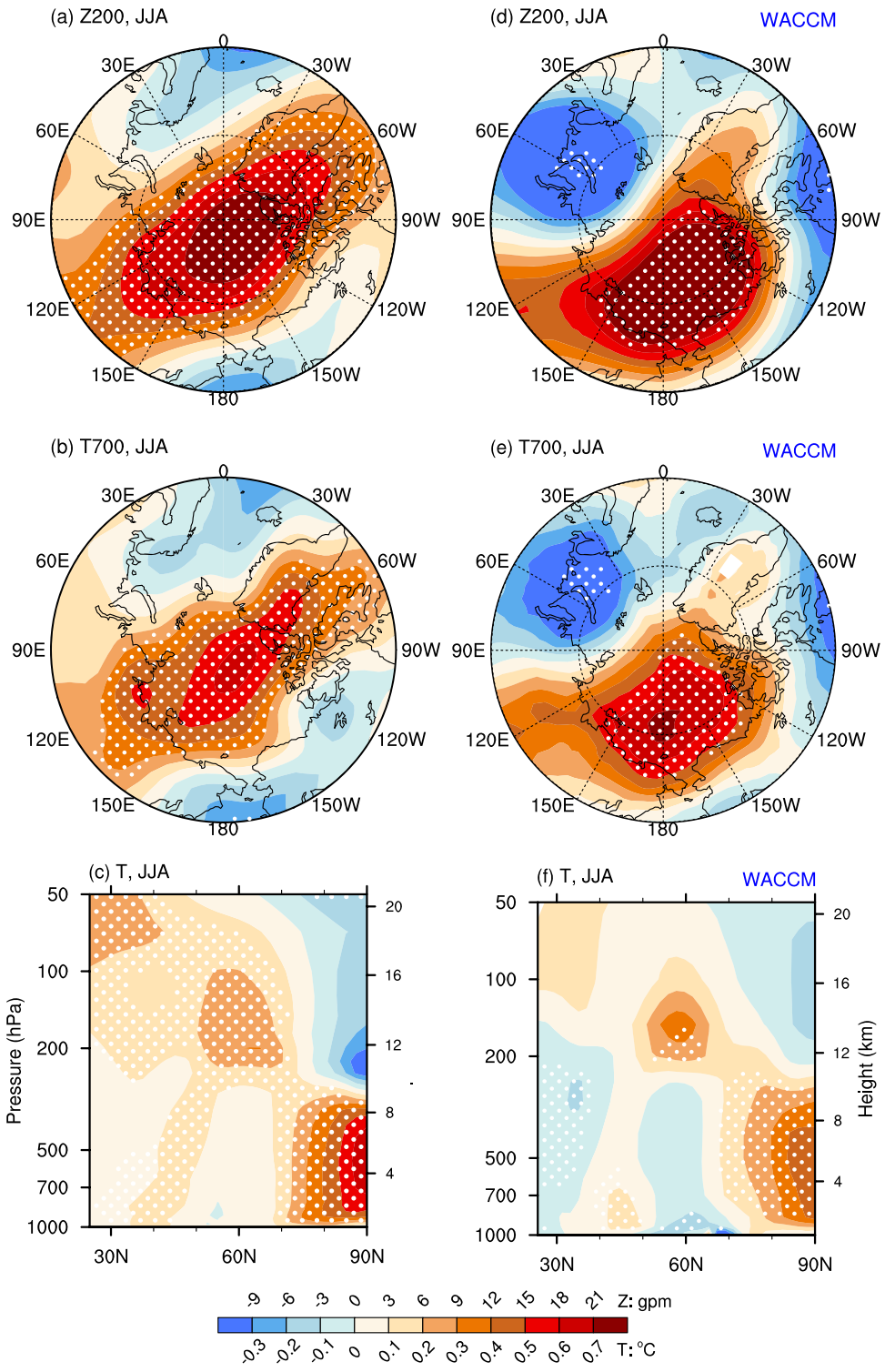

Fig. 5. Impacts of North Pacific SST on the Arctic warming. Regression of (a) 200-hPa geopotential height (Z200; shading; units: gpm), (b) 700-hPa temperature (T700; shading; units: °C), and (c) air temperature zonally averaged along 180°–150°W (*T*; shading; units: °C) for JJA 1979–2022 related to the detrended and normalized May ENPSSTI. Shading in (a) and hatching in (b, c) indicate anomalies statistically significant at the 0.05 level. Panels (d–f) are the same as (a–c), respectively, but for the differences between the ensemble mean of sensitivity runs and control runs by WACCM.

these teleconnections are mainly derived from wintertime (November–March) or annual mean datasets. In contrast to previous studies, our results demonstrate that the summer Arctic atmospheric circulation can be influenced by the extratropical North Pacific SST. These results are parallel to Li et al. (2015) who suggested the influence of winter extratropical ocean warming on the winter Arctic sea ice and atmospheric circulation.

Funding

This research was supported by the National Natural Science Foundation of China [Grants No. 41991283], the Research Council of Norway Funded Project BASIC [Grant No. 325440], and Chinese–Norwegian Collaboration Projects Within Climate funded by the Research Council of Norway (COMBINED) [Grant No. 328935].

Acknowledgments

High-performance computing and storage resources were performed on resources provided by Sigma2— the National Infrastructure for High Performance Computing and Data Storage in Norway (through project NS8121K). NCEP/DOE Reanalysis II can be downloaded from https://psl.noaa.gov/data/gridded/data.ncep.reanalysis2.html. HadISST1 data were obtained from the Met Office Hadley Centre website at https://www.metoffice.gov.uk/hadobs/hadisst/.

References

Bromwich, D.H., Fogt, R.L., Hodges, K.I., Walsh, J.E., 2007. A tropospheric assessment of the ERA-40, NCEP, and JRA-25 global reanalyses in the polar regions. J. Geophys. Res. Atmos. 112, D10111.
Chylek, P., Folland, C.K., Lesins, G., Dubey, M.K., Wang, M., 2009. Arctic air temperature change amplification and the Atlantic Multidecadal Oscillation. Geophys. Res. Lett. 36, L14801.
Collow, T.W., Wang, W.Q., Kumar, A., 2017. Simulations of Eurasian winter temperature trends in coupled and uncoupled CFSv2. Adv. Atmos. Sci. 35, 14–26.
Dai, A., Luo, D., Song, M., Liu, J., 2019. Arctic amplification is caused by sea-ice loss under increasing CO_2. Nat. Commun. 10, 121.
Day, J., Hargreaves, J., Annan, J., Abe-Ouchi, A., 2012. Sources of multi-decadal variability in Arctic sea ice extent. Environ. Res. Lett. 7, 034011.
Deser, C., Teng, H., 2008. Evolution of Arctic sea ice concentration trends and the role of atmospheric circulation forcing, 1979–2007. Geophys. Res. Lett. 35, 7–26.
Ding, Q., Schweiger, A., Baxter, I., 2022. Nudging Observed winds in the arctic to quantify associated sea ice loss from 1979 to 2020. J. Clim. 35, 3197–3213.
Ding, Q., Schweiger, A., L'Heureux, M., Battisti, D.S., Po-Chedley, S., Johnson, N.C., Blanchard-Wrigglesworth, E., et al., 2017. Influence of high-latitude atmospheric circulation changes on summertime Arctic sea ice. Nat. Clim. Chang. 7, 289–295.
Ding, Q., Wallace, J.M., Battisti, D.S., Steig, E.J., Gallant, A.J., Kim, H.J., Geng, L., 2014. Tropical forcing of the recent rapid Arctic warming in northeastern Canada and Greenland. Nature 509, 209–212.
Gerber, F., Sedláček, J., Knutti, R., 2014. Influence of the western North Atlantic and the Barents Sea on European winter climate. Geophys. Res. Lett. 41, 561–567.
Hu, A., Rooth, C., Bleck, R., Deser, C., 2002. NAO influence on sea ice extent in the Eurasian coastal region. Geophys. Res. Lett. 29 (22), 2053.
IPCC, 2013. Climate change 2013: The physical science basis. Contribution of Working Group I to the fifth assessment report of the intergovernmental Panel on Climate Change. Cambridge University Press, Cambridge, United Kingdom and New York, NY, USA, p. 1535.
IPCC, 2022. Climate change 2022: Impacts, adaptation, and vulnerability. Contribution of Working Group II to the sixth assessment report of the Intergovernmental Panel on Climate Change. Cambridge University Press. Cambridge University Press, Cambridge, UK and New York, NY, USA, p. 3056.
Kanamitsu, M., Ebisuzaki, W., Woollen, J., Yang, S.K., Hnilo, J., Fiorino, M., Potter, G., 2002. Ncep-doe amip-ii reanalysis (r-2). Bull. Am. Meteorol. Soc. 83, 1631–1644.
Knudsen, E.M., Orsolini, Y.J., Furevik, T., Hodges, K.I., 2015. Observed anomalous atmospheric patterns in summers of unusual Arctic sea ice melt. J. Geophys. Res. Atmos. 120, 2595–2611.
Lapointe, F., Francus, P., Lamoureux, S.F., Vuille, M., Jean-Philippe, J., Bradley, R.S., Massa, C., 2017. Influence of North Pacific decadal variability on the western Canadian Arctic over the past 700 years. Clim. Past 13, 411–420.
Li, F., Wang, H., Gao, Y., 2015. Extratropical ocean warming and winter Arctic sea ice cover since the 1990s. J. Clim. 28, 5510–5522.
Lind, S., Ingvaldsen, R.B., Furevik, T.J.N.C.C., 2018. Arctic warming hotspot in the northern Barents Sea linked to declining sea-ice import 8, 634–639.
Lindsey, R., and Scott, M., 2022. Climate change: Arctic sea ice summer minimum. [Available online at https://www.climate.gov/news-features/understanding-climate/climate-change-arctic-sea-ice-summer-minimum].
Lindzen, R., Farrell, B., 1980. A simple approximate result for the maximum growth rate of baroclinic instabilities. J. Atmos. Sci. 37, 1648–1654.
Mantua, N.J., Hare, S.R., Zhang, Y., Wallace, J.M., Francis, R.C., 1997. A Pacific interdecadal climate oscillation with impacts on salmon production. Bull. Am. Meteorol. Soc. 78, 1069–1079.
Marsh, D.R., Mills, M.J., Kinnison, D.E., Lamarque, J.-F., Calvo, N., Polvani, L.M., 2013. Climate change from 1850 to 2005 simulated in CESM1 (WACCM). J. Clim. 26, 7372–7391.
Matsumura, S., Yamazaki, K., 2012. Eurasian subarctic summer climate in response to anomalous snow cover. J. Clim. 25, 1305–1317.
Matsumura, S., Zhang, X., Yamazaki, K., 2014. Summer Arctic atmospheric circulation response to spring Eurasian snow cover and its possible linkage to accelerated sea ice decrease. J. Clim. 27, 6551–6558.
McCusker, K.E., Fyfe, J.C., Sigmond, M., 2016. Twenty-five winters of unexpected Eurasian cooling unlikely due to Arctic sea-ice loss. Nat. Geosci. 9, 838–842.
Moore, G., 2012. Decadal variability and a recent amplification of the summer Beaufort Sea High. Geophys. Res. Lett. 39, L10807.
Ogi, M., Wallace, J.M., 2007. Summer minimum Arctic sea ice extent and the associated summer atmospheric circulation. Geophys. Res. Lett. 34, L12705.
Overland, J.E., Wang, M., 2010. Large-scale atmospheric circulation changes are associated with the recent loss of Arctic sea ice. Tellus A 62, 1–9.
Overland, J.E, Francis, J.A, Hanna, E, Wang, M, 2012. The recent shift in early summer Arctic atmospheric circulation. Geophys. Res. Lett 39, L19804.
Peings, Y., Magnusdottir, G., 2014. Forcing of the wintertime atmospheric circulation by the multidecadal fluctuations of the North Atlantic ocean. Environ. Res. Lett. 9, 034018.
Rayner, N.A., Parker, D. E., Horton, E. B., Folland, C. K., Alexander, L. V., Rowell, D. P., Kent, E. C., Kaplan, A., 2003. Global analyses of sea surface temperature, sea ice, and night marine air temperature since the late Nineteenth Century. J. Geophys. Res. Atmos. 108, 1063–1082.
Rigor, I.G., Wallace, J.M., Colony, R.L., 2002. Response of sea ice to the Arctic oscillation. J. Clim. 15, 2648–2663.
Screen, J.A., Deser, C., Simmonds, I., 2012. Local and remote controls on observed Arctic warming. Geophys. Res. Lett. 39, L10709.
Serreze, M.C., Barrett, A.P., 2008. The summer cyclone maximum over the central Arctic ocean. J. Clim. 21, 1048–1065.
Serreze, M.C., Barry, R.G., 2011. Processes and impacts of Arctic amplification: A research synthesis. Glob. Planet. Chang. 77, 85–96.
Serreze, M.C., Barrett, A.P., 2011. Characteristics of the Beaufort Sea high. J. Clim. 24, 159–182.
Stroeve, J., Holland, M.M., Meier, W., Scambos, T., Serreze, M., 2007. Arctic sea ice decline: Faster than forecast. Geophys. Res. Lett. 34, L09501.
Svendsen, L., Keenlyside, N., Bethke, I., Gao, Y., Omrani, N.-E., 2018. Pacific contribution to the early twentieth-century warming in the Arctic. Nat. Clim. Chang. 8, 793–797.
Swart, N.C., Fyfe, J.C., Hawkins, E., Kay, J.E., Jahn, A., 2015. Influence of internal variability on Arctic sea-ice trends. Nat. Clim. Chang. 5, 86–89.
Takaya, K., Nakamura, H., 2001. A formulation of a phase-independent wave-activity flux for stationary and migratory quasigeostrophic eddies on a zonally varying basic flow. J. Atmos. Sci. 58, 608–627.
Trenberth, K.E., Fasullo, J.T., Branstator, G., Phillips, A.S., 2014. Seasonal aspects of the recent pause in surface warming. Nat. Clim. Chang. 4, 911–916.
Watanabe, E., Wang, J., Sumi, A., Hasumi, H., 2006. Arctic dipole anomaly and its contribution to sea ice export from the Arctic Ocean in the 20th century. Geophys. Res. Lett. 33, L23703.
Xu, J., Luo, J.J., Yuan, C., 2022a. Tropical indian ocean warming contributes to Arctic warming. Geophys. Res. Lett. 49, e2022GL101339.
Xu, X., He, S., Zhou, B., Wang, H., 2022b. Atmospheric Contributions to the reversal of surface temperature anomalies between early and late winter over Eurasia. Earth's Future 10, e2022EF002790.
Zhang, X., Ikeda, M., Walsh, J.E., 2003. Arctic sea ice and freshwater changes driven by the atmospheric leading mode in a coupled sea ice–ocean model. J. Clim. 16, 2159–2177.
Zhang, X., Sorteberg, A., Zhang, J., Gerdes, R., Comiso, J.C., 2008. Recent radical shifts of atmospheric circulations and rapid changes in Arctic climate system. Geophys. Res. Lett. 35, L22701.